ELSEVIER

A computational investigation of unsteady separated flows

P. Koutmos and C. Mavridis
Department of Mechanical Engineering, University of Patras, Patras, Greece

This work describes the computational investigation of unsteady separated flow configurations periodic, quasi-periodic or flapping within the framework of a global approach. A two-dimensional (2D) time-dependent Navier–Stokes procedure was formulated, which encompasses aspects from both the large-eddy simulation (LES) formalism and the conventional k-ε procedures. Within this context, an effort is made to distinguish large-scale active structures both on the basis of their character—deterministic or random—as well as on their size while taking into account the percentage contribution of the vortical structure energy in the total fluctuating energy budget. The proposed model was successfully applied to the calculation of such unsteady separated flow configurations as square cylinder wake and backward-facing step recirculating flows under low- and high-Reynolds number conditions. © 1997 by Elsevier Science Inc.

Keywords: cylinder wake flow; backward-facing step flow; modified eddy-viscosity models; vortex-shedding flow

Introduction

Unsteady separated flow regions have numerous engineering applications in addition to their fundamental significance (Bearman 1984; Laurence and Mattei 1993). A separated shear layer created by the detachment of a uniform flow may dynamically reattach and redevelop on a constraining surface (backward-facing step configuration, Driver and Seegmiller 1985) or freely roll-up into large-scale alternating vortices (bluff-body vortex-shedding flow; Lyn 1989). Good understanding of these complex turbulent flows is necessary to improve methods of prediction (Kato and Launder 1993; Deng et al. 1993; Lasher and Taublee, 1992; Jakirlic and Hanjalic 1994) and to allow better control (Oertel 1990; Roos and Kegelman 1986) or exploitation (Igarashi 1985) of their dynamic features.

Several studies (Bearman 1984; Lyn 1989; Driver and Seegmiller 1985; Driver et al. 1987; Leder and Geropp 1990; Le et al. 1993) have provided detailed information on the separation region of generic configurations. These efforts have greatly aided in the development of Navier–Stokes (N–S) solvers and turbulence models currently used for the efficient design of technical systems involving flows with high- or low-level large-scale unsteadiness. Recent studies (Kato and Launder 1993; Deng et al. 1993, Lasher and Taulbee 1992) using the Reynolds- (or ensemble-) averaged N—S equations (RANS/EANS) have shown that such important design parameters as shedding frequencies, drag and lift coefficients, reattachment positions, and skin friction losses may be reasonably predicted provided there is a fixed detachment position. The superiority of large-eddy simulations (LES) over EANS when details of the flows are sought has, nonetheless, been clearly demonstrated (Murakami et al. 1993), but cost increases in CPU time and storage are on the order of 10 or 100.

Alternatively, within the context of EANS procedures, whether using an eddy-viscosity model, (EVM) or second-moment closure (SMC), it is necessary to clarify the ambiguity concerning a possible overlap between the resolved and the modeled part of the three-dimensional (3D) turbulence. The nondimensional time-scale of the unsteadiness may not be sufficiently separate from the time-scale of turbulence to justify use of time-averaged solutions (Lasher and Taulbee 1992); partitioning may be inadequate even when adopting a two-dimensional (2D) EANS procedure (Laurence and Mattei 1993). Although LES procedures may address this aspect more effectively, economic routine parametric studies in industrial applications are still required, and this warrants the continued testing of conventional models in a range of unsteady separated flows.

In the present work, a 2-D hybrid time-dependent Navier–Stokes model is formulated that blends aspects from both the LES formalism and the conventional k-ε procedures. Within this framework, an attempt is made to analyse unsteady separated flows consistently (with periodic, quasi-periodic, or flapping motion) with a global approach. Flows where unsteadiness is organized and present as the larger part of the total fluctuation energy (e.g., cylinder wake), as well as flows where lower-frequency quasi-periodic fluctuations are recognized as a low-level contributor to the total energy (e.g., backstep flows) may then be handled through a common procedure. Within the present treatment, a distinction is made of the structures based both on their character (deterministic or random) as well as on their size. The simple Smagorinsky (1963) model combined with a standard k-ε model are coupled to the low-Re wall method of Rodi et al. (1993) to calculate the mean and unsteady behavior of square cylinder and back-step flows. For the first configuration,

Address reprint requests to Prof. P. Koutmos, Department of Mechanical Engineering, University of Patras, Patras, Rio 26500, Greece.

Received 21 June 1995; accepted 11 July 1996

Int. J. Heat and Fluid Flow 18: 297–306, 1997

655 Avenue of the Americas, New York, NY 10010

0142-727X/97/$17.00
PII S0142-727X(97)00009-X

as a basis for comparison, laser-Doppler velocimetry (LDV) measurements of the mean and turbulent wakes are obtained from Bakrozis et al. (1994) for Re = 8520 and 14,285 (blockage = 19%) and from Lyn (1989) for Re = 22,000 (blockage = 7%). For the second study, data from Driver and Seegmiller (1985), Driver et al. (1987), and Le et al. (1993) are used. Comparisons between calculations and measurements indicated the potential of the "mixed" method to reproduce most features of the complex unsteady flows covered in the experiments.

Flow configuration

The cylinder configuration chosen as the first test case is shown in Figure 1a. In Bakrozis et al. (1994), the 8-mm model was inserted into a 6:1 aspect ratio rectangular cross-sectional duct of 42-mm height, thus producing an area blockage of 0.19. Detailed measurements have been obtained for this configuration for two Reynolds numbers of 8520 and 14,285 based on cylinder diameter and approach velocity. These data were chosen, because they were obtained under significant confinement, thus supplementing previous investigations (Kato and Launder, 1993; Deng et al. 1993) and also were available at two different Reynolds numbers. Uniform axial velocity profiles were measured 4.5D upstream of the cylinder with HWA over 85% of the span with about 1% turbulence levels. Profiles of the mean axial and cross-stream velocities together with corresponding turbulent intensities and statistics are available throughout the wake region and were obtained with a one-component 2-W A–I laser-Doppler velocimeter operated with standard TSI optics. Further details on the experiments may be found in Bakrozis et al. (1994). Computations were also performed for a square cylinder flow with 7% blockage and a Reynolds number of 22,000, for which detailed data have been reported by Lyn (1989).

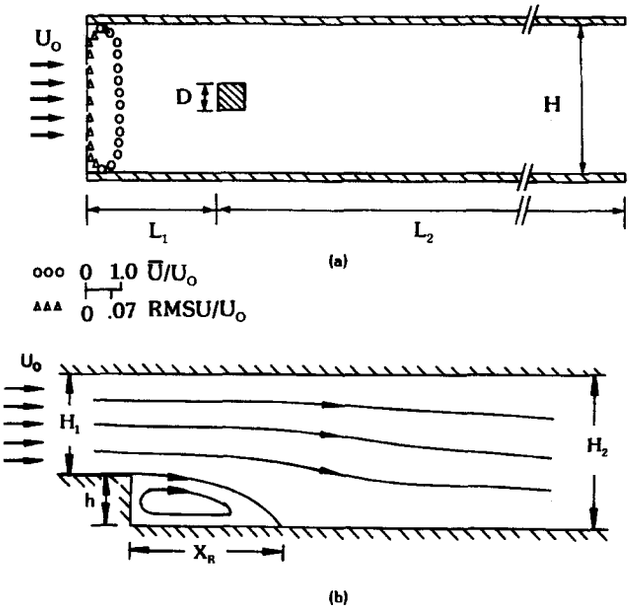

Figure 1 a) Square cylinder flow configuration; b) backward-facing step flow configuration

The second test case is the back-step flow (Figure 1b) where large-scale vortex development occurs under wall-bounding conditions. Whilst in the previous flow, large-scale, unsteady vortical structures are responsible for the largest percentage of apparent shear stress in the total energy budget (Franke and Rodi 1991), in the back-step, this contribution has been identified at a much

Notation

B	blockage factor, D/H
C_D	drag coefficient
C_f	skin friction coefficient
C_S	Smagorinsky's model coefficient
C_P	pressure coefficient
C_μ	turbulent viscosity coefficient
D	square cylinder diameter
$E(n)$	contribution to $\langle u^2 \rangle$ *in frequency band* Δn $\langle u^2 \rangle = \int_0^\infty E(n)\,dn = \int_{-\infty}^{+\infty} nE(n)d[\log(n)]$
f	frequency
F(n)	contribution of $\langle p^2 \rangle$ in frequency band Δn $\langle p^2 \rangle = \int_0^\infty F(n)\,dn = \int_{-\infty}^{+\infty} nE(n)d[\log(n)]$
h	step height
H	channel height
k	turbulence kinetic energy
L	turbulent length scale
N	number of samples for the evaluation of flow statistics
M	number of intervals dividing each periodic cycle
n	nondimensional frequency ($n = fX_R/U_o$)
u, v, w	velocities
U_o	approach flow velocity
P	static pressure
Re	Reynolds number Re = $U_o D/\nu$ or $U_o h/\nu$
S_t	Strouhal number
S_{ij}	strain rate tensor
t_o	charactristic nondimensional flow time-scale (D/U_o or h/U_o)
x_i	coordinate directions ($i = 1,2,3$)
x_R	time-averaged reattachment location

Greek

δ_{ij}	*Kronecker delta* ($\delta_{ij} = 0$ *for* $i \neq j$; $\delta_{ij} = 1$ *for* $i = j$)
Δ	characteristic mesh size
ε	turbulence energy dissipation rate
λ	[stochastic (unresolved) fluctuation energy]/(total fluctuation energy), (Equation 5)
ν	molecular viscosity
ν_t	eddy-viscosity coefficient
ρ	density

Subscripts

i	$i = 1,2,3$ Cartesian coordinate
i, j, k	tensor notation
t	turbulent flow, total
c	explicitly (statistically) evaluated
p	periodic component

Superscripts

+	wall coordinates

Operators

$\langle\ \rangle$	ensemple-averaged (resolved) quantity
$(-)$	time-averaged
$(\ )''$	Large-scale (resolved) fluctuation
$(\ )'$	Turbulent (subgrid) fluctuation

lower level (Driver et al. 1987). These selected cases represent a rigorous test of the model's ability to reproduce a diversity of unsteady separated flows. The measurements of Driver and Seegmiller (1985) and Jovic and Driver as reported in Le et al. (1993) were used for comparisons. These were performed at two Reynolds numbers of 5000 and 37,000 and at low-expansion ratios of 1.2 and 1.125, which are a more stringent check of a model's ability to reproduce this flow.

Numerical method

Formulation

The unsteady, separated flows were calculated by solving the 2-D time-dependent (ensemble-averaged) N–S equations governing the temporal and spatial variation of the velocities and pressures

$$u = \langle u \rangle + u' \qquad \text{with} \qquad \langle u \rangle = \bar{u} + u'' \tag{1}$$

where u and $\langle u \rangle$ are the instantaneous and ensemble-averaged (resolved) velocities, $\bar{u}$ and u'' the time-mean and large-scale (resolved) fluctuating components, and u' the random (subgrid) turbulent fluctuation. The model closely follows the formulation adopted in Koutmos and Mavridis (1994). The equation set may be expressed as follows:

$$\frac{\partial \langle u_i \rangle}{\partial x_i} = 0$$

$$\frac{\partial \langle u_i \rangle}{\partial t} + \langle u_j \rangle \frac{\partial \langle u_i \rangle}{\partial x_j} = -\frac{1}{\rho}\frac{\partial p}{\partial x_i} + \frac{\partial}{\partial x_j}\left(\nu \frac{\partial \langle u_i \rangle}{\partial x_j} - \langle u_i' u_j' \rangle\right) \tag{2}$$

The ensemble-averaged products of velocity fluctuations or Reynolds stresses are here obtained from the eddy-viscosity formula:

$$-\langle u_i' u_j' \rangle = \langle \nu_t \rangle \left(\frac{\partial \langle u_i \rangle}{\partial x_j} + \frac{\partial \langle u_j \rangle}{\partial x_i}\right) - \frac{2}{3}\langle k \rangle \delta_{ij} \tag{3}$$

In the standard k-ε model $\langle \nu_t \rangle$ is related to the turbulence energy $\langle k \rangle$ and its dissipation $\langle \varepsilon \rangle$; i.e.,

$$\langle \nu_t \rangle = c_\mu \frac{\langle k \rangle^2}{\langle \varepsilon \rangle} \tag{4}$$

where $\langle k \rangle$ and $\langle \varepsilon \rangle$ are obtained from their standard transport equations (see Kato and Launder 1993).

The k-ε model has been calibrated to "reproduce" the spectrum of plain shear flows (with no distinct peaks). When a 2-D, time-dependent calculation is used, part of the spectrum is resolved by the main solution itself. If the standard k-ε is simply adopted for ensemble-averaged turbulent quantities, an overlap of the resolved and modeled parts may result, and this may lead to a wrong specification of ν_t. This approach (coupled to the one-equation low-Re wall method of Rodi et al. 1993) produced, in the cylinder flow computations (Re = 8520), irregular shedding with an increased period by about 20%, underestimation of back-flow velocities by 50% and lengthening of the vortex by 20%. It is unclear whether this modeling approach correctly partitions the total stress into its stoachastic and periodic contributions. The Smagorinsky model ($C_s = 0.1$) was also employed within the 2-D procedure and reduced the shedding period by 16%, while it underestimated vortex length and strength by 17% and 30%, respectively. A further computation with no-turbulence model ($\nu_t = 0$) resulted in somewhat higher underpredictions than the Smagorinsky model.

In the present time-dependent procedure, the spatial filtering due to the mesh employed is also accounted for in an effort to distinguish the directly computed 2-D turbulent motions, which are resolved by the mesh of size $\Delta (= (\Delta x \Delta y)^{1/2})$, from the turbulence already modeled and represented by the k-ε model. The eddy-viscosity is evaluated by borrowing the Smagorinsky model (or any other model, such as that of Neto et al. 1993), and the formulation is as follows:

$$\langle \nu_t \rangle = (C_s \Delta)^2 (2\langle S_{ij} \rangle \langle S_{ij} \rangle)^{1/2} + \lambda c_\mu \frac{\langle k^2 \rangle}{\langle \varepsilon \rangle}$$

$$\text{if} \qquad L = \frac{\langle k \rangle^{3/2}}{\langle \varepsilon \rangle} > \Delta$$

and

$$\langle \nu_t \rangle = c_\mu \frac{\langle k \rangle^2}{\langle \varepsilon \rangle} \qquad \text{if} \qquad L < \Delta \tag{5}$$

C_s was here taken as 0.1. This choice was not found to be critical, however, because the variable λ factor takes into account the need for a variable C_s. $\lambda = \bar{k}/\bar{k}_t$, where $\bar{k}$ is the time-averaged value of $\langle k \rangle$ statistically obtained from the k-ε as the solution progressed in time. $\bar{k}_t$ is the time-averaged total fluctuation energy (modeled + resolved) equal to $\bar{k}_c + \bar{k}$ and $\bar{k}_c$ is the resolved fluctuation energy recovered by the time-dependent procedure and is evaluated as:

$$\bar{k}_c = \frac{1}{2}(U_{\text{rms},c}^2 + V_{\text{rms},c}^2)$$

with

$$U_{\text{rms},c} = \left[\frac{1}{N}\sum_{i=1}^{N}(\langle u_i \rangle - \bar{u})^2\right]^{1/2},$$

$$V_{\text{rms},c} = \left[\frac{1}{N}\sum_{i=1}^{N}(\langle V_i \rangle - \bar{V})^2\right]^{1/2} \tag{6}$$

N is the number of samples in the flow statistics and $U_{\text{rms,c}}$ and $V_{\text{rms,c}}$ are the fluctuations resolved by the numerical procedure.

For a given time-dependent solution and grid resolution, $\bar{k}_c$ contains the periodic energy component $\bar{k}_p$ and additional purely stochastic (but resolved) 2-D turbulent contributions ($\bar{k}'$). This would lead to some ambiguity as to which portion of the total fluctuation energy would be modeled if the full k-ε was used and whether k-ε is applied correctly, because the constants were, in any case, tuned for steady-state flows. The periodic component, $\bar{k}_p$ here is directly calculated from the periodic components $U_{\text{rms,p}}$, and $V_{\text{rms,p}}$. These are obtained from the solution by identifying the cycle repetition (e.g., via a pressure signal), dividing the cycle into intervals, and averaging over each interval and repeated cycles. The phase-averaging procedure produces values $\langle u \rangle_{pi}, \langle v \rangle_{pi}$ ($i = 1$ to M, where M is the number of cycle intervals) used in Equation 6 to obtain the periodic intensities. Both $\bar{k}$

and $\bar{k}_c$ were cumulatively (statistically) obtained as the solution progressed in time to gradually produce the correct level of the parameter λ.

In the present form, the ensemble-averaged decomposition corresponds physically to a two-level distinction and classification of the structures. At the first level, their deterministic or random character (i.e., whether they are resolved by the mesh or not) is identified by implicitly comparing their physical scales with the mesh scale of size Δ. At the second, their *k-ε modeled* scales are explicitly compared with the mesh scale in an effort to apportion the correct level of eddy-viscosity to the unresolved portion of the stochastic fluctuations. The mixed model performed better than the standard *k-ε* or the pure Smagorinsky; the percentage the mixed model is turned on is typically 70 to 80% in the cylinder flows. The $\langle \nu_t \rangle$ resulting from Equation 5 (and not the standard expression $C_\mu \langle k \rangle^2 / \langle \varepsilon \rangle$) is also used in the production of $\langle k \rangle$, in the *k-ε* equations. This gradually produces a continuous distribution of $\langle \nu_t \rangle$ and avoids inconsistencies in the boundaries between the regions where the mixed or the standard $\langle \nu_t \rangle$ expressions are turned on. The internal iteration per time-step, within the employed implicit scheme, is well suited for this hybrid formulation. The above model also helped to obviate the need for a special treatment of the turbulence energy production to avoid unrealistic overshoots of $\langle k \rangle$ in the cylinder's forward stagnation point (Kato and Launder 1993); the mixed $\langle \nu_t \rangle$ component is switched on in this region ($\lambda \approx 0.3$). The evaluation of the total time-averaged rms U and V values, which are compared with the measurements, is proceeding through the simple anisotropic model (Friedrich and Nieuwstadt 1994):

$$U_{i,\mathrm{rms}} = \left(U^2_{i,\mathrm{rms},c} + \left(\frac{u^2_{i,\mathrm{rms},c}}{0.5(1+a)(U^2_{\mathrm{rms},c} + V^2_{\mathrm{rms},c})} \right) \bar{k} \right)^{1/2} \qquad \text{with} \quad i = 1,2 \quad (7)$$

Because of the 2-D nature of the approach, an assumption was introduced for the $W_{\mathrm{rms},c}$ component; i.e., $W^2_{\mathrm{rms},c} = a(U^2 + V^2)_{\mathrm{rms},c}$. According to literature surveys by Ruderich and Fernholz (1986) for the step flows, a is here given a value of 0.45; the LES studies of Murakami et al. (1993) suggest that a value of 0.2 may be appropriate for the cylinder flow. It should be stressed that these are tentative values and necessary only because of the imposed restrictions of the 2-D approach. A similar assumption ($a = 0.2$) has been introduced in the estimation of k_{tot} for the present cylinder flow measurements because only the U and V rms components were measured.

Apportioning the turbulent fluctuating energy amongst its components similarly to the partition of the resolved tensor in Equation 7 is justified by the results and discussion of Goutorbe et al. (1994). These authors demonstrated remarkably similar energy distributions amongst the components of the resolved and modeled tensors with the help of DNS. In a subsequent LES study, they modeled with some success the subgrid-scale (SGS) stress tensor proportionately to the resolved tensor rather than the strain tensor.

Numerical details

For the cylinder flows, the calculation domain extended from $4.5D$ upstream to $25D$ downstream of the cylinder. Three meshes were used of $79 \times 65, 157 \times 121$, and 201×175 (x, y) grid points, and the second mesh with clustering near the body was found to produce an acceptable level of refinement and accuracy for engineering purposes and was used for all presented results. Minimum cell sizes (normalised with D) were of the order of 3–5%, and the expansion ratios used downstream of the formation region were 1.1 to 1.175. For the backstep, the solution domain covered from $10h$ upstream to $25h$ downstream of the step for the $\mathrm{Re} = 5000$ case. For the $\mathrm{Re} = 37{,}000$ case, the downstream domain was extended up to $60h$. Two meshes comprising 160×80 and 220×120 (x, y) grid points were used for the low- and high-Re case, respectively. One reviewer quite correctly noted that, because the grid size regulates the evaluation of the eddy-viscosity, the results for a given mesh cannot be termed as grid-independent in the usual sense. Grid-refinement, however, can be undertaken to reduce the discretisation errors.

The method described in the Formulation section was coupled to the *k-ε*-based, one-equation, low-Re model of Rodi et al. (1993), which was adopted for all near-wall regions. Within the two-layer model practice, the standard high-Re *k-ε* form is retained in the core region, while in viscosity dominated wall regions, the k equation is still solved, but the ε equation is replaced by a simple algebraic expression of the form $\varepsilon = (V/L_\varepsilon)^* f_\varepsilon$. L_ε is a dissipation length scale, f_ε is a damping function required to give a nonzero ε value at the wall, and V is a velocity scale. A different length scale L_μ is now used for the determination of the turbulent viscosity as $\nu_t = V^* L_\mu$. This wall model uses different slopes for L_ε and L_μ (see Rodi et al.), which are determined from DNS data and replaces $k^{1/2}$ with $(\bar{v}^2)^{1/2}$ as the velocity scale V. The standard *k-ε* and the two-layer component are matched at a position where $\nu_t/\nu = 16$. In the grids used, 3–8 points, depending upon location, participated in the two-layer model.

In-flow conditions for the cylinder were specified in accordance with the mean and turbulent profiles measured at 4.5D upstream of the body. To simulate the inlet profile for the step as close as possible to the experimental and DNS conditions, a boundary layer was first computed, and solutions were marched downstream to reach the experimentally reported Re_θ numbers at the quoted position. The profiles of velocities and turbulence quantities corresponding to the present inlet axial position were then used as inlet conditions. At the outlet, the simple convective boundary condition:

$$\frac{\partial u_i}{\partial t} + c\frac{\partial u_i}{\partial x} = 0 \qquad (\mathrm{c} = \text{mean channel velocity}) \quad (8)$$

was implemented and reduced the time required to achieve vortex-shedding conditions.

The system of the coupled partial differential equations was solved by using a finite-volume scheme based on a staggered mesh, a pressure correction method (SIMPLE), and the QUICK differencing scheme. Further details of the solution method may be found in Koutmos (1985). A three-level-backward implicit Euler second-order scheme (Deng et al. 1993) was used for temporal discretisation. Typical time-steps were of the order 10^{-4}–10^{-5} s depending on Reynolds number and retained a Courant number below 0.35. All runs were performed on an HP735 Risc System, and typical run times for a shedding cycle in the cylinder flow were about 2 h. Flow statistics are evaluated after the initial transient at about $t = 50D/u_o$.

Results and discussion

The hybrid model results are compared with experimentally available time-mean data and statistical quantities, and the performance of the present method is appraised and discussed.

Figures 2 and 3 show the measured and calculated time-averaged axial velocity and fluctuating (periodic turbulent, $\bar{k}_t$) energy distributions along the cylinder symmetry plane for the two Reynolds numbers of 8520 and 14,285. A time-averaged vortex length of 0.94D with back-flow velocities up to 30% of the approach velocity accompanied by a wake development within

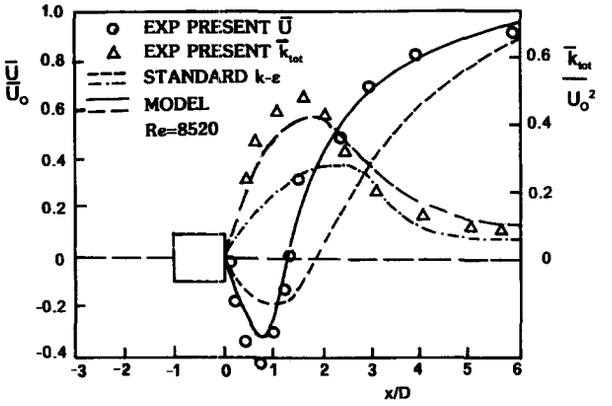

Figure 2 Development of time-averaged streamwise velocity and total fluctuating energy along symmetry plane (Re= 8520, $D/H=0.19$)

5D is observed in both measurements and calculations for the higher Re number case. At the lower Re number, both predictions and experiment indicate an increase of about 35% in maximum mean blackflow velocities and recirculation lengths. A similar trend with Re number has been found in the quasi-LES (no subgrid model was used at the higher Re numbers) of circular cylinders by Tamura et al. (1990). The enhanced entrainment found in the lower Re case is accompanied by an increase in peak turbulence levels of about 20%. This trend as well as the positions and levels of the turbulence energy peaks at the forward stagnation point have been captured well by the hybrid method. Standard k-ε computations using the same one-equation, near-wall model are also displayed in the Figures and are clearly inferior to the predictions of the present method.

Time-averaged axial and transverse mean velocities and turbulence intensities for a location half-way through the formation region are shown in Figure 4. In both measurements and calculations, peak mean and rms V means of order 40 and 100% of U_o, respectively, are observed near the forward stagnation point as a consequence of its more energetic participation in the unsteady wake development. Overall, the agreement was satisfactory throughout the near- and far-wake locations for both Re numbers.

As a further test of the model's performance, the square cylinder flow of Lyn (1989) was calculated next. These measure-

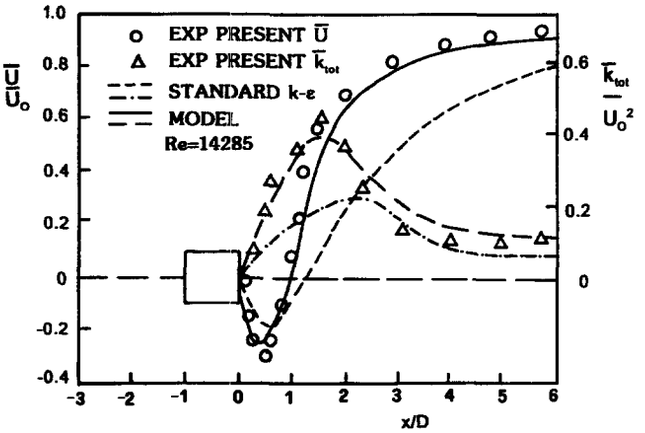

Figure 3 Development of time-averaged streamwise velocity and total fluctuating energy along symmetry plane (Re= 14,285, $D/H=0.19$)

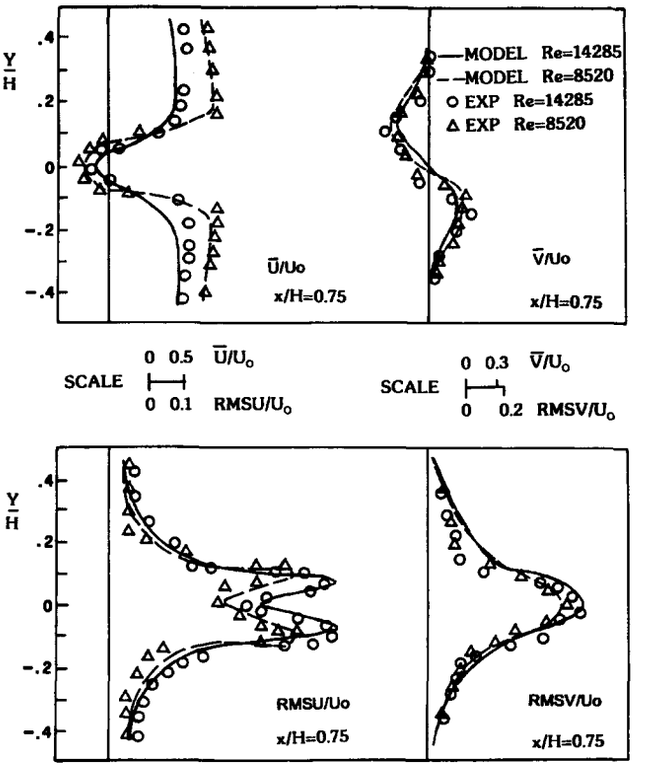

Figure 4 Time-averaged mean and rms streamwise and cross-stream velocity distributions at two Reynolds numbers for the square cylinder flow ($D/H=0.19$)

ments were obtained with a much smaller blockage (7%), at a higher Re number (Re = 22,000) and have been a standard test case thus far. Predictions with the present model are included below and allow a valuable comparison with reported work. Turbulence intensities (TU) of 0.8, 0.9, and 2% [with $k/U_o^2 = 3/2(\mathrm{TU})^2$] were used as inlet conditions for the above three consecutive Re number computations. Measured profiles were utilised for the prediction of the present experiments, while a uniform inlet distribution was used for the Re = 22,000 case. Inlet dissipation rates were obtained from k values assuming a length scale equal to 1/4 of the tunnel height. The measured and computed time-averaged axial velocity and total fluctuating energy ($\bar{k}_t$) along the symmetry plane are shown in Figure 5,

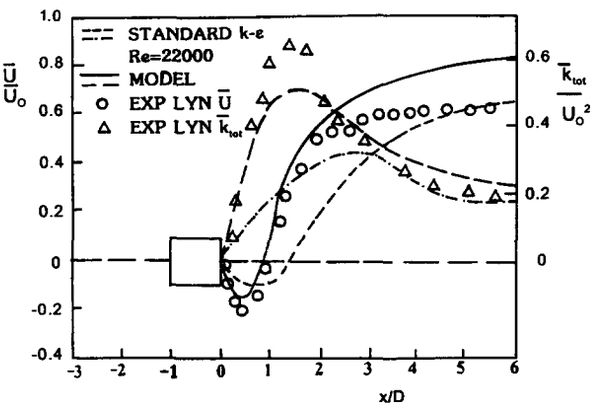

Figure 5 Development of time-averaged axial velocity and total fluctuating energy along symmetry plane (Re=22,000, $D/H=0.07$)

while similar distributions for the turbulent ($\bar{k}_c - \bar{k}_p + \bar{k}$) and periodic ($\bar{k}_p$) energies are displayed in Figure 6. These comparisons demonstrate an equally satisfactory model performance and a correct partition of the stochastic and periodic energy components. It seems from Figure 6 that the contribution of the resolved stochastic fluctuations ($k_c - k_p$) is rather large. These are 2-D fluctuations, and the question arises as to whether a 2-D approach represents this energy properly, because the mechanism of vortex stretching is essentially 3-D. A comparison with a 3-D solution would, therefore, be useful. Similarly, the computed vortex street conforms well to the measured trend, as shown in Figure 7, although its "amplitude" and "wave length" are underestimated.

The symmetry plane distributions depicted in Figures 2, 3, 5, and 6 have frequently been used as a diagnostic for various CFD methods of this vortex-shedding flow (Kato and Launder 1993; Rodi (1993). The present method circumvented some of the difficulties encountered in previous k-ε computations (particularly in the region up to $x/D = 3$) giving an indication of the capability of the formulated combination. The above mean velocity predictions are comparable to the 3-D LES results of Murakami et al. (1993) and are inferior to the computation of Deng et al. (1993) in the region downstream of $x/D = 3$. This latter work used the Baldwin–Lomax model, which basically produced appreciable eddy-viscosity levels only in the cylinder wall vicinity. However, their results with or without the above mixing length model were very close, leading to the impression that numerical diffusion alone would be sufficient to describe the turbulence in this flow. To the contrary, this study found that numerical damping alone is inadequate. The mixed model, nonetheless, reproduced, to a significant extent, the experimentally determined Re number dependence and blockage effect in both the mean and rms values as illustrated in Figures 2, 3, 5, and 6.

The alternating vortex shedding is better illustrated in Figure 8 in the form of streaklines for various phases for the Re = 14,285 case. The two vortices formed on the cylinder flanks are gradually intensified and consecutively occupy the main recirculation. This unsteady character emerges in the calculated axial velocity power spectra displayed in Figure 9 for both Reynolds numbers, which also compare satisfactorily with measurements.

Computed integral parameters such as Strouhal numbers and drag coefficients closely correspond with present measurements and literature values (Table 1). Strouhal and drag coefficient values obtained here for a blockage of 19% are about 30 and 12% higher than those reported by Lyn (1989) and Murakami et al. (1993) for a blockage of 7% implying the influence of this parameter. When the geometrically "blocked" velocity past the cylinder is used rather than the inlet velocity the resulting

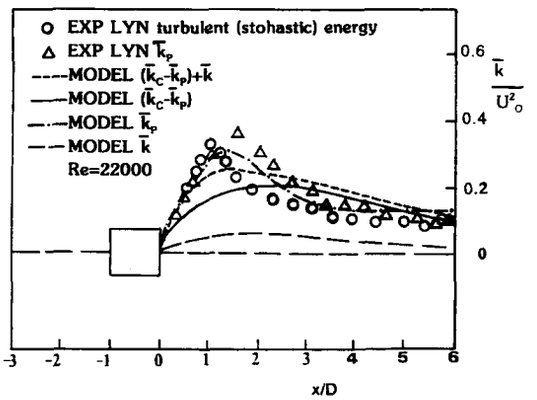

Figure 6 Time-averaged turbulent and periodic energy distributions along the symmetry plane

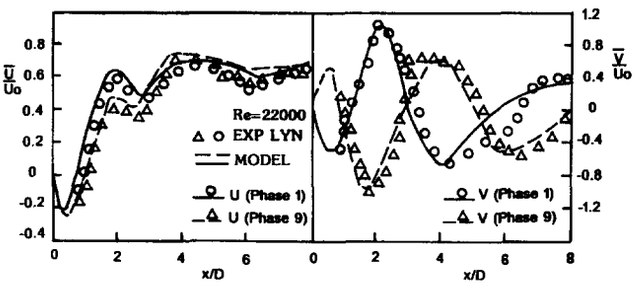

Figure 7 Axial and normal velocities along symmetry plane for two phases

Strouhal (= 0.14) agrees better with literature values for lower blockage. Nevertheless it should be stressed that this does not provide an equivalent "zero-blockage" result. The use of the one-equation, low-Re model was also conducive to the successful prediction of these parameters; initial computations with wall functions resulted in discrepancies of more than 25%.

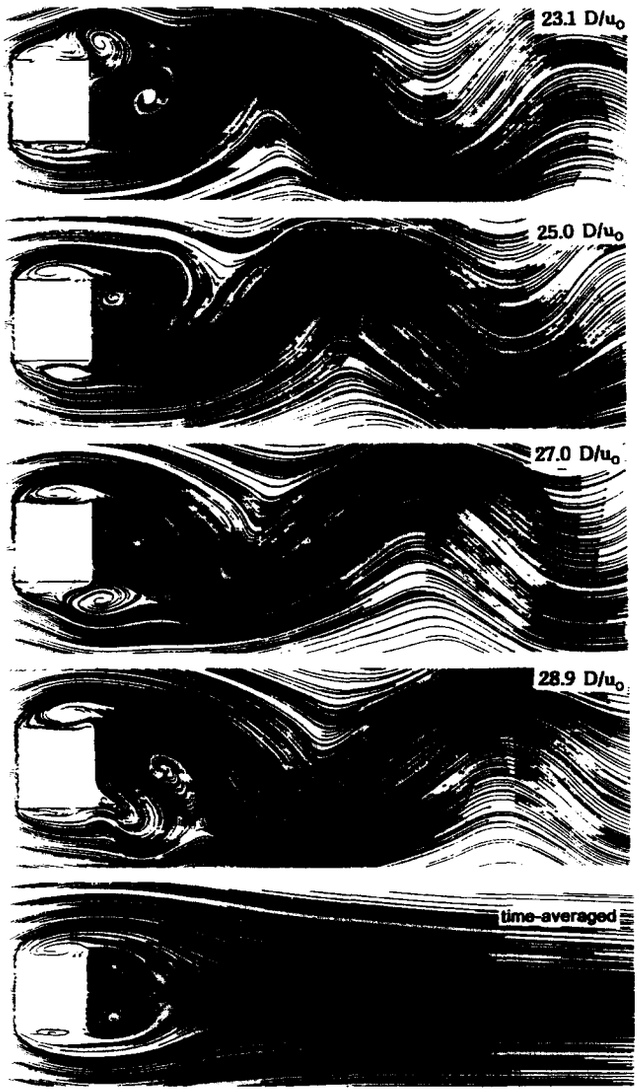

Figure 8 Phase and time-averaged streaklines for the cylinder flow at Re=14,285, (D/H=0.19)

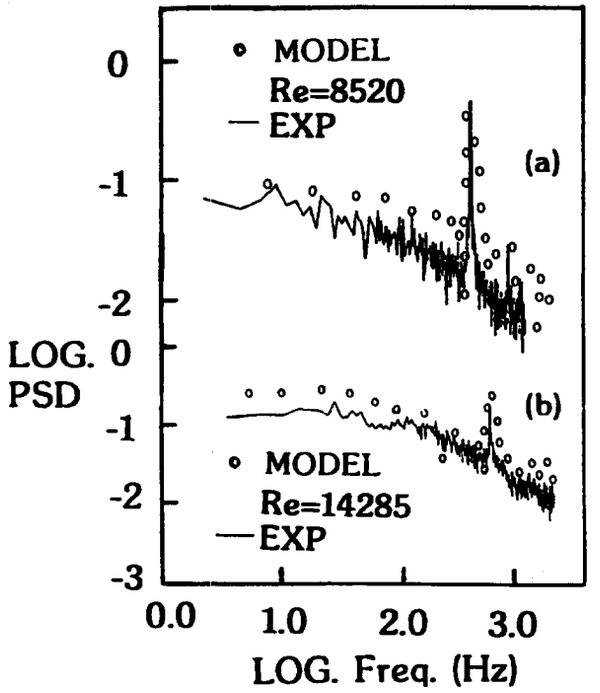

Figure 9 U velocity power spectra at $(x/D, y/D)=(3,0)$ for square cylinder flow at Re=14,285, Re=8520 ($D/H=0.19$)

The two back-step configurations were subsequently computed with the same model. The time-averaged flow details are presented first, while the predicted quasi-periodic behaviour (as opposed to the harmonic unsteadiness seen in the cylinder flow) are discussed later.

Figures 10a, b display the overall development in the form of streaklines for the high (Re = 37,000 and ER = 1.125) and low (Re = 5000, ER = 1.2) Re number cases, respectively. These 2-D, time-dependent back-step flow calculations generated solutions that maintained unsteadiness of the separated flow, especially near reattachment for both Re numbers. For the lower Re number case, additional streakline patterns at two different times through the computation, corresponding to $t = 46.3$ (h/U_o) and 52.1 (h/U_o) are shown as an example in Figure 10b. A quasi-periodic behaviour with the separation bubble exhibiting short and long reattachments in a similar fashion as observed experimentally by Driver et al. (1987) emerged in these solutions. Reattachment and corner eddy lengths of $6h$ and $1.5h$ were calculated for the former case, which are close to the experimental values. For the lower Re case, respective values were computed at $5.95h$ and $0.5h$, again, in line with measured lengths.

Table 1 Comparison of present computations with literature

	S_t	C_D
Exp. present Re=14,285, $D/H=0.19$	0.176	—
Exp. present Re=8520, $D/H=0.19$	0.178	—
Present model Re=14,285, $D/H=0.19$, 157×121	0.178	2.37 ± 0.20
Present model Re=8520, $D/H=0.19$, 157×121	0.180	2.37 ± 0.20
Exp. Iyn Re=22,000, $D/H=0.07$	0.135	2.14 ± 0.09
Present model Re=22,000, $D/H=0.07$, 157×121	0.139	2.09 ± 0.10

Figures 11 and 12 compared measured and calculated profiles of mean and fluctuating velocities (obtained from Equation 7) and turbulence kinetic energy at various stations through the recirculation and redevelopment regions for the two Re numbers. Within the recirculation (Figures 11, 12, $x/h=4$), good agreement is observed with maximum discrepancies of 20–35% found in the rms. It is encouraging to affirm satisfactory agreement at station $x/h=6$ (Figures 11, 12), located at the edge of the recirculation region, thus emphasizing the importance of adequately reproducing the reattachment length within the context of any calculation method suitable for this flow. Further along at stations $x/h=8,12,20$ (Figure 11) and $x/h=10$ (Figure 12), as the flow redevelops downstream of reattachment, predictions are also in satisfactory agreement with measurements.

As indicated in Figure 11, the resolved 2-D fluctuation energy levels are, at most, 17% of the total; in comparison to the cylinder flow (Figure 6), large-scale unsteadiness here contributes to the total energy to a much lesser extent. The k-ϵ model component is now much more dominant and contributes significantly to the evaluation of the eddy-viscosity. The values of the λ factor, discussed below, provide further evidence on this.

Figures 13a and b present measured and calculated friction factors and wall static pressure coefficients. For the high Re case, predicted peak negative values in the recirculation region, for both the c_f and c_p distributions, are shifted upstream. The predicted c_f recovery is slower than the measured, although beyond $x/h=20$, the correct level is finally reached. For Re = 5000, predictions overshoot by about 12% the minimum c_f and c_p values, but in both cases, the recovery slopes are quite satisfactory.

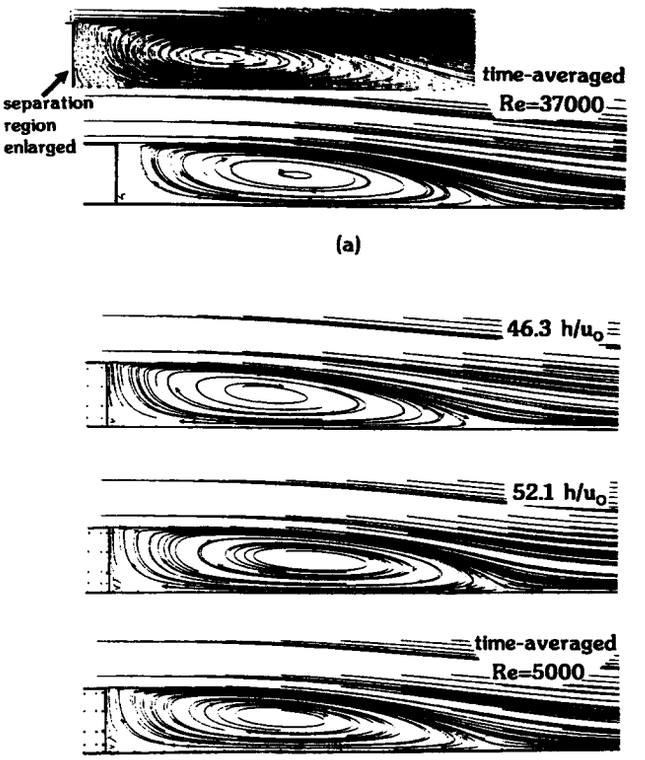

Figure 10 Computed phase and time-averaged streamlines for the two backstep flow configurations

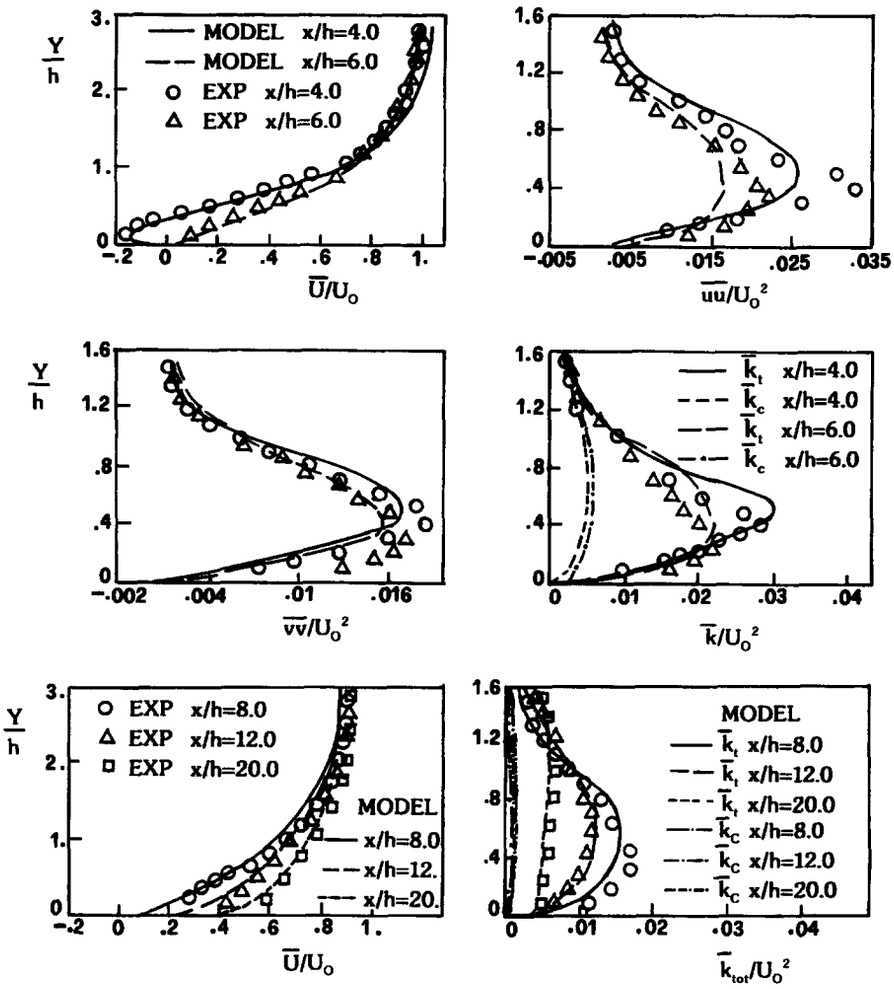

Figure 11 Comparisons between calculated and measured profiles for the backstep flow at various axial positions for Re=37,000

From the above comparisons, the picture that emerges is that the present formulation has proved efficient throughout the complex flow regions encountered in this configuration. The results suggest that the time-dependent mixed model has performed better than other models in reported steady-state backstep calculations, even when some second-moment closures were used (Lasher and Taulbee 1992; Sindir 1983). Such a favourable comparison implies that the present formulation performs consistently both under equilibrium and nonequilibrium conditions. Along with the above remarks, we should note that a steady-state solution may also be suitable, to a large extent, for this type of flow. Very successful steady-state step flow solutions have been obtained by employing an anistropic nonlinear eddy-viscosity model (Thangam and Speziale 1992). Therefore, more advanced models of this type, such as that of Craft et al. (1995) may be even more suitable, and it would be quite interesting to apply them within a time-dependent frame to properly resolve any large-scale unsteady features in this flow. Such an approach may be necessary for step flows involving shear-layer excitation (Roos and Kegelman 1986) or other forms of active flow control. The intention is to apply the present hybrid model to such types of flows as well.

Overall, we should notice that the pure k-ε prevailed near the walls (e.g., cylinder flanks, channel, and step walls), in shear layers with steep velocity gradients, and in reattachment positions. Typical distributions of the λ factor for the two geometries are shown in Figure 14. λ values in the cylinder flow were less than 20%, with the lower levels found in the wake formation region where the percentage contribution of the large-scale unsteady vortical structures in the total energy is maximum. Oppositely, in the step flow, λ values were greater than 70–80%, with the bottom range occurring near the reattachment position. As the grid was refined or the Reynolds number was lowered, the pure k-ε contribution was seen to gradually decrease.

Measured and calculated energy spectra of the surface static pressure at $x/h = 5.5$ and of the axial velocity at $x/h = 6$, $y/h = 1$ compare favourably in Figures 15a and b. As in the experiments, the functions $F(n)$ and $E(n)$ represent the fraction of the total mean-square pressure and velocity fluctuations, respectively, in a band width $\Delta n = 0.01$. In Figure 15, $(nF(n))^{1/2}$ and $nE(n)$ are plotted against the normalised frequency $n = fx_R/U_o$. Most of the predicted energy resides around the nondimensional frequency $n = 0.56$, while in the experiments, the corresponding value is 0.6. The existence of a band of frequencies with increased energy and the lack of a discrete and pronounced value implies the active role played by a range of eddy sizes in these resolved large-scale unsteady motions and signifies the quasi-periodic character of the flow (Lasher and Taulbee 1992). On the other hand, as pointed by the reviewers, this resolved band lies much higher than the "very-low-frequency" values usually associated with large shear-layer eddies; no evidence of these low values are, in fact, provided in the spectral results of the present solution.

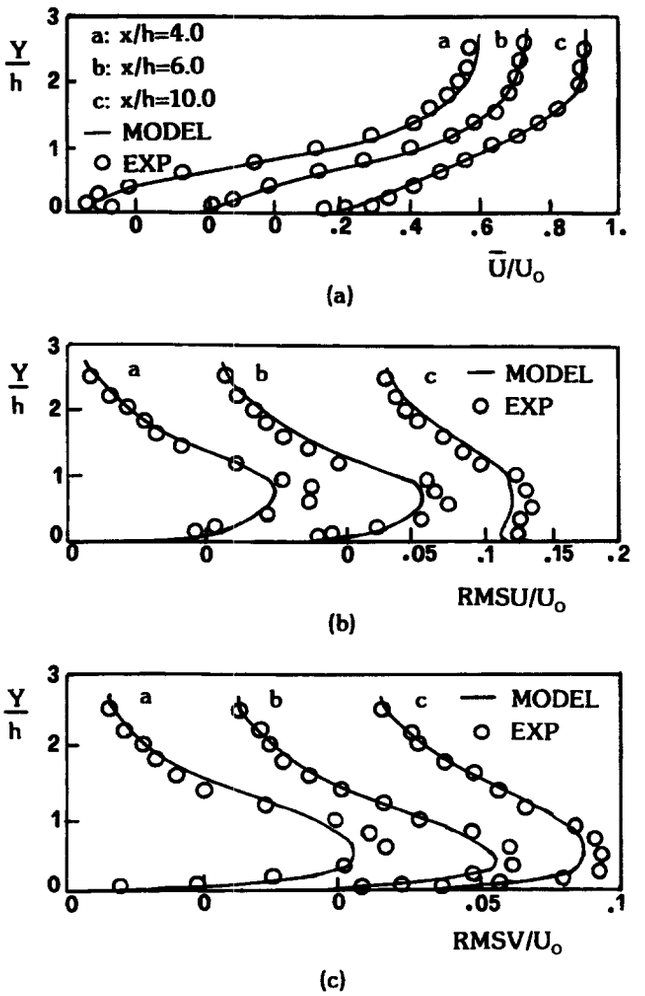

Figure 12 Comparisons between calculated and measured profiles for the backstep flow at various axial positions for Re=5000

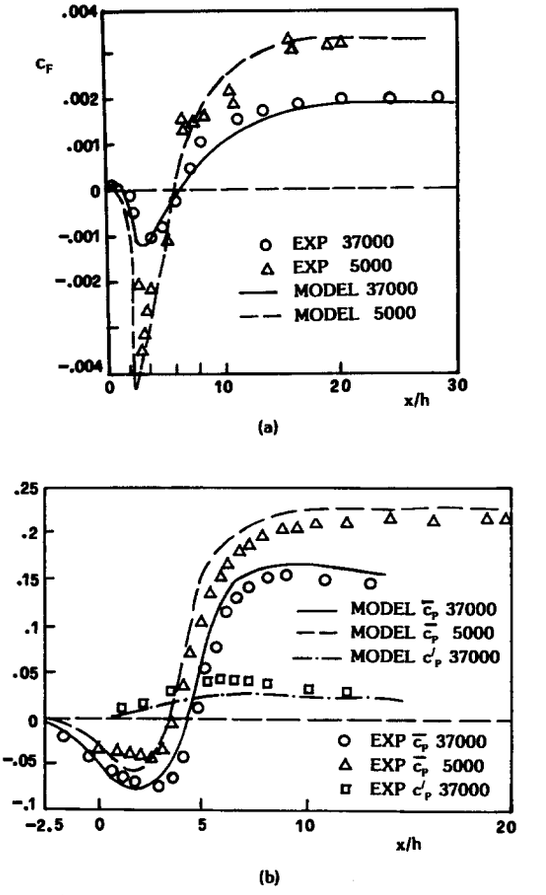

Figure 13 Comparisons between measured and calculated skin friction and wall static pressure coefficients for Re= 37,000, Re=5000

Conclusion

A hybrid 2-D, time-dependent Navier–Stokes model has been formulated that blends elements from both the LES methodology and the standard eddy-viscosity approaches. Within this framework, an effort was made to consistently analyse unsteady separated flows, periodic or quasi-periodic within the context of a global approach. Large-scale active vortex structures are, hereby, characterized both by their quality—deterministic or random—as well as by their size. The model was tested by application to a range of unsteady, separated flows such as square cylinder wakes and backward-facing steps, where large-scale vortical structures are present as low- or high-level contributors to the total fluctuation energy.

Detailed comparisons between calculations and measurements underlined the ability of the same model form to cope satisfactorily with the variety of complex unsteady flow phenomena found in the experiments. Vortex lengths, shedding frequencies, skin friction, and pressure coefficients, as well as the detailed velocity and turbulence fields of these flows were calculated adequately for a range of Reynolds numbers. For the cylinder flows, the "mixed" model clearly outperformed standard k-ε procedures and produced results of similar quality to some reported second-moment closure solutions. For the back-step flows, the present time-dependent formulation improved on results obtained by steady-state standard k-ε closures. It also provides a suitable methodology for the study of flows with an externally imposed unsteadiness. Further detailed tests and refinements of the described method may be required for other classes of engineering flows to demonstrate and verify its applicability.

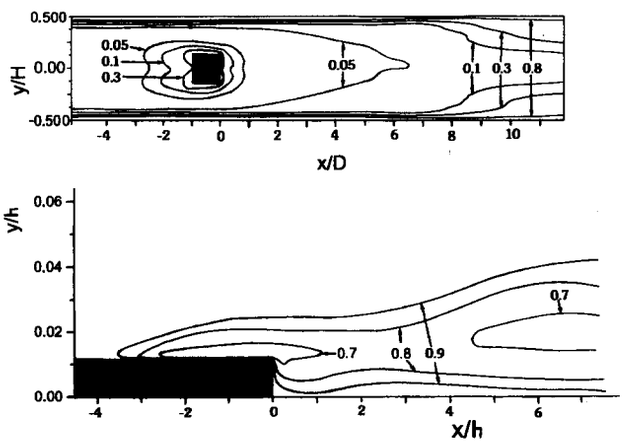

Figure 14 Typical distributions of the λ factor for a) cylinder flow and, b) backstep flow

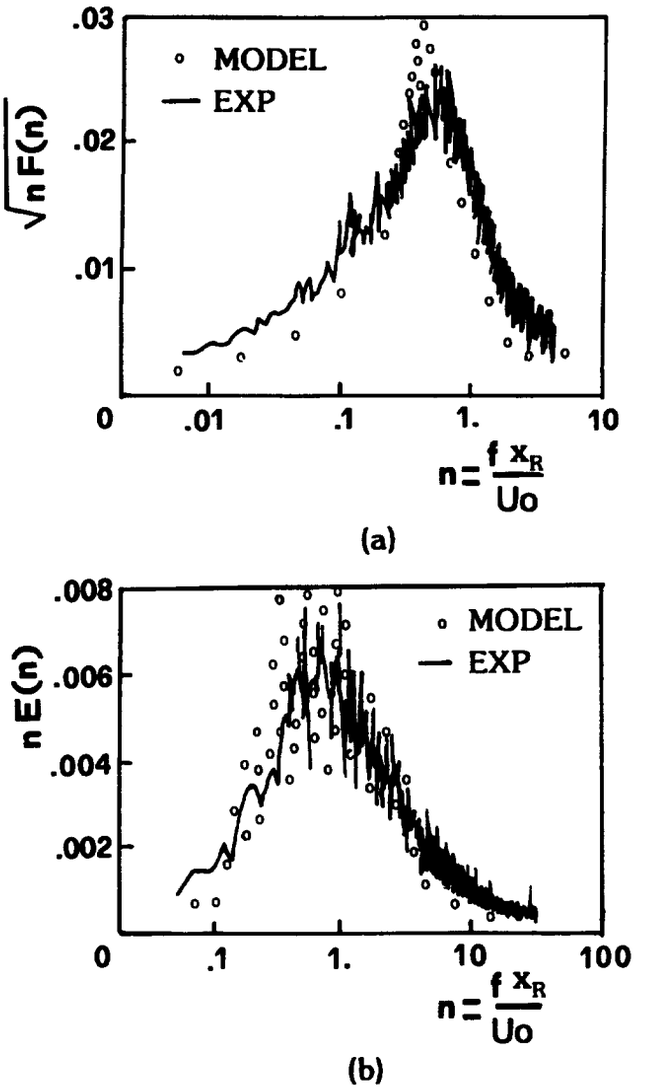

Figure 15 Comparisons between measured and calculated energy spectra at Re=37,000 for a) wall static pressure at $x/h=5.5$ and b) axial velocity at $(x/h, y/h)=(6, 1)$

References

Bakrozis, A. Koutmos, P. and Papailiou, D. 1994. Experimental investigation of unsteady square cylinder turbulent wake flows. *Lab. Appl. Thermodynamics*. University of Patras, Patras, Rio, Greece, Rep. LAT-EXP-JOU1

Bearman, P. W. 1984. Vortex shedding from oscillating bluff bodies. *Ann. Rev. Fluid Mech.*, **16**, 195–222

Craft, T. J., Launder, B. E. and Suga, K. 1995. A non-linear eddy-viscosity model including sensitivity to stress anisotropy. *Proc. 10th Symp. on Turbulent Shear Flows*, The Pennsylvania State University, University Park, Pa, Paper 23–19

Deng, G. B., Piquet, J., Quentey, P. and Visonneau, M. 1993. Flow past a square cylinder: Predictions with an eddy-viscosity model. *Proc. 9th Symp. on Turbulent Shear Flows*, Kyoto, Japan, Paper 16–18

Driver, D. M. and Seegmiller, H. L. 1985. Features of a reattaching turbulent shear layer in divergent channel flow. *AIAA J.*, **23**, 163–171

Driver, D. M., Seegmiller, H. L. and Marvin, J. G. 1987. Time-dependent behavior of a reattaching shear layer. *AIAA J.*, **25**, 914–919

Franke, R. and Rodi, W. 1991. Calculation of vortex shedding past square cylinder with various turbulence models. *Proc. 8th Symp. on Turbulent Shear Flows*, Munich, Germany, Paper I–2

Friedrich, R. and Nieuwstadt, F. T. M. 1994. LES of pipe flow. ERCOFTAC bulletin No. 22, Sept. 1994

Goutorbe, T., Laurence, D. and Maupu, V. 1994. An priori test of an SGS tensor model including anisotropy and backscatter effects. In *Direct and Large-Eddy Simulation I*, Voke et al. (eds.), Kluwer Academic, Norwell, MA, 121–131

Igarashi, T. 1985. Fluid flow around a bluff-body used for Karman vortex flowmeter. *Proc. Int. Symp. on Fluid Control and Measurements, FLUCOME 86*, Tokyo, Japan, 1017–1022

Jakirlic, S. and Hanjalic, K. 1994. On the performance of the second-moment high- and low-Re- number closures in reattaching flows. *Proc. Int. Symp. on Turbulence, Heat and Mass Transfer*, 9–12 August, Lisbon, Portugal

Kato, M. and Launder, B. E. 1993. The modeling of turbulent flow around stationary and vibrating square cylinders. *Proc. 9th Symp. on Turbulent Shear Flows*, Kyoto, Japan, Paper 10–4

Koutmos, P. (1985). An isothermal study of gas turbine combustor flows. *Ph.D. thesis*, University of London, London, UK

Koutmos, P. and Mavridis, C. 1994. Numerical investigation of unsteady square cylinder wake flows with and without 2D central jet injection. *Lab. Applied Thermodynamics*, University of Patras, Patras, Rio, Greece, Rep. LAT-CFD-LESI

Lasher, W. C. and Taoulbee, D. B. 1992. On the computation of turbulent backstep flows. *Int. J. Heat Fluid Flow*, **13**, 30–40

Laurence, D. and Mattei, J. D. 1993. Current state of computational bluff body aerodynamics. *J. Wind Eng. Ind. Aero.*, **49**, 23–44

Le, H., Moin, P. and Kim, J. 1993. Direct numerical simulation of turbulent flow over a backward-facing-step. *Proc. 9th Symp. on Turbulent Shear Flows*, Kyoto, Japan, Paper 13–2

Leder, A. and Geropp, D. 1990. Dynamics of turbulent energy production in separated flows. *Proc. 1st Symp. on Eng. Turb. Modelling and Measurements*, Sept. 24–28, Dubrovnik, Yungoslavia

Lyn, D. A. 1989. Phase-averaged turbulence measurements in the separated shear layer region of flow around a square cylinder. *Proc. 23rd Congress of the Int. Ass. Hyd. Research*, Ottawa, Ont., Canada, pp. A85–A92

Murakami, S. 1993. Comparison of various turbulence models applied to a bluff-body. *J. Wind Eng. Ind. Aero.*, **46, 47**, 21–36

Murakami, S., Rodi, W., Mochida, A. and Sakamoto, S. 1993. LES of turbulent vortex shedding flow past 2D square cylinder. *Proc. ASME Fluids Eng. Conference*, Washington, DC

Neto, A. S., Grand, D., Metails, O. and Lesieur, M. 1993. A numerical investigation of the coherent vortices in turbulence behind a backward-facing step. *J. Fluid Mech.*, **256**, 1–25

Oertel, H. 1990. Wakes behind bluff bodies. *Ann. Rev. Fluid Mech.*, **22**, 539–564

Roos, F. and Kegelman, J. T. 1986. Control of coherent structures in reattaching laminar and turbulent shear layers. *AIAA J.*, **24**, 1956–1963

Rodi, W. 1993. On the stimulation of turbulent flow past bluff-bodies. *J. Wind Eng. Ind. Aero.*, **46, 47**, 3–19

Rodi, W., Mansour, N. N. and Michelassi V. 1993. One-equation near-wall turbulence modeling with the aid of direct simulation data. *J. Fluids Eng.*, **115**, 196–208

Ruderich, R. and Fernholz, H. H. 1986. An experimental investigation of a turbulent shear flow with separation, reverse flow and reattachment. *J. Fluid Mech.*, **163**, 283–322

Sindir, M. M. 1983. Effects of expansion ratio on the calculation of parallel-walled backward-facing-step flows: Comparison of four models of turbulence. ASME Paper 83-FE-10

Smagorinsky, J. 1963. General circulation experiments with the primitive equations: I. The basic experiment. *Monthly Weather Rev.*, **91**, 99–112

Tamura, T., Ichiro, T. and Kuwahara, K. 1990. On the reliability of two-dimensional simulations for unsteady flows around a cylinder-type structure. *J. Wind. Eng. Ind. Aero.*, **32**, 275–298

Thangam, S. and Speziale, C. G. 1992. Turbulent flow past a back-facing step: A critical evaluation of two-equation models. *AIAA J.* **30**, 1314–1320